

Highly Conductive Bilayer Transparent Conducting Oxide Thin Films for Large-Area Organic Photovoltaic Cells

Jun Liu,[†] Alexander W. Hains,[†] Jonathan D. Servaites,[‡] Mark A. Ratner,^{*,†,‡} and Tobin J. Marks^{*,†,‡}

[†]Department of Chemistry and [‡]Department of Materials Science and Engineering, Argonne-Northwestern Solar Energy Research Center and the Materials Research Center, Northwestern University, Evanston, Illinois 60208-3113

Received July 23, 2009. Revised Manuscript Received September 24, 2009

Highly conductive In-doped CdO/Sn-doped In_2O_3 (CIO/ITO) bilayer transparent conducting oxide (TCO) thin films were prepared by combining, in sequence, metal-organic chemical vapor deposition (MOCVD) and ion-assisted deposition (IAD) techniques. The bilayer substrates, with a low In content of ~19 atom % and a low sheet resistance of only $\sim 4.9 \Omega/\square$, were investigated as anodes in the bulk-heterojunction (BHJ) organic photovoltaic (OPV) devices using poly(2-methoxy-5-(3',7'-dimethyloctyloxy)-1,4-phenylenevinylene) (MDMO-PPV):[6,6]-phenyl C_{61} butyric acid methyl ester (PCBM) as the active layer. The bilayer anode OPVs of the current laboratory size ($\sim 0.06 \text{ cm}^2$) exhibit performance comparable to those of commercial ITO-based control devices. The effect of TCO conductivity on OPV performance in larger area devices is analyzed through a simulation model. The results reveal significant advantages of using the highly conductive bilayer TCO anodes for large-area OPV cells.

Introduction

Organic photovoltaic (OPV) devices, with the attraction of low cost, lightweight, efficient roll-to-roll fabrication and compatibility with flexible substrates, have been intensively investigated over the past decade.^{1–7} Bulk-heterojunction (BHJ) OPV devices typically consist of a polymer donor + fullerene acceptor blend as the active layer, sandwiched between two contacting electrodes. Upon illumination, charge carriers are generated in the active layer by exciton dissociation and are subsequently collected at the electrodes. While a low work function metal is typically utilized as the electron-collecting cathode, a transparent conducting oxide (TCO) film is generally used as the hole-collecting anode, for which Sn-doped In_2O_3 (ITO) with a conductivity of 3000–5000 S/cm and visible range transparency of $\sim 85\%$ is almost universally employed. However, the modest ITO conductivity and soaring In prices render ITO a less-than-optimum choice for future applications. Thus, TCOs with

greater conductivity and transparency, and with lower In content, would be highly desirable.^{8–11}

Among those physical parameters that affect OPV device performance, the cell series resistance (R_s), also known as the internal resistance, is one of the most important and typically arises from three contributions: (1) bulk resistances of the active layer and interfacial layers, (2) contact resistances at the interfaces, and (3) resistances of the electrodes.^{12,13} Since the cathode metals usually have several orders of magnitude higher conductivities than the anode TCOs, the R_s portion due to electrode resistances arises predominantly from the anode TCO resistance, R_{s-TCO} . It is physically reasonable that R_{s-TCO} should have an increasingly significant effect on device performance as device area increases, and thus large-area OPV should more evidently benefit from more conductive TCOs. However, to date, such an effect has not been quantified on the basis of experimental results.

We report here the application of a highly conductive In-doped CdO (CIO)/ITO bilayer TCO as the anode in

*To whom correspondence should be addressed. E-mail: ratner@northwestern.edu, t-marks@northwestern.edu.

- (1) Tang, C. W. *Appl. Phys. Lett.* **1986**, *48*, 183.
- (2) Krebs, F. C. *Sol. Energy Mater. Sol. Cells* **2009**, *93*, 394.
- (3) Kroon, R.; Lenes, M.; Hummelen, J. C.; Blom, P. W. M.; De Boer, B. *Polym. Rev.* **2008**, *48*, 531.
- (4) Gunes, S.; Neugebauer, H.; Sariciftci, N. S. *Chem. Rev.* **2007**, *107*, 1324.
- (5) Park, S. H.; Roy, A.; Beaupre, S.; Cho, S.; Coates, N.; Moon, J. S.; Moses, D.; Leclerc, M.; Lee, K.; Heeger, A. J. *Nat. Photonics* **2009**, *3*, 297.
- (6) Irwin, M. D.; Buchholz, B.; Hains, A. W.; Chang, R. P. H.; Marks, T. J. *Proc. Natl. Acad. Sci. U.S.A.* **2008**, *105*, 2783.
- (7) Hains, A. W.; Marks, T. J. *Appl. Phys. Lett.* **2008**, *92*, 023504.

- (8) Fortunato, E.; Ginley, D.; Hosono, H.; Paine, D. C. *MRS Bull.* **2007**, *32*, 242.
- (9) Ni, J.; Yan, H.; Wang, A. C.; Yang, Y.; Stern, C. L.; Metz, A. W.; Jin, S.; Wang, L.; Marks, T. J.; Ireland, J. R.; Kannewurf, C. R. *J. Am. Chem. Soc.* **2005**, *127*, 5613.
- (10) Ni, J.; Wang, L.; Yang, Y.; Yan, H.; Jin, S.; Marks, T. J.; Ireland, J. R.; Kannewurf, C. R. *Inorg. Chem.* **2005**, *44*, 6071.
- (11) Martin, E. J. J.; Yan, M.; Lane, M.; Ireland, J.; Kannewurf, C. R.; Chang, R. P. H. *Thin Solid Films* **2004**, *461*, 309.
- (12) Sze, S. M.; Ng, K. K. *Physics of Semiconductor Devices*; John-Wiley & Sons, Inc.: Hoboken, NJ, 2007.
- (13) Green, M. A. *Solar Cells: Operating Principles, Technology, and System Applications*; Prentice-Hall Inc.: Englewood Cliffs, NJ, 1982.

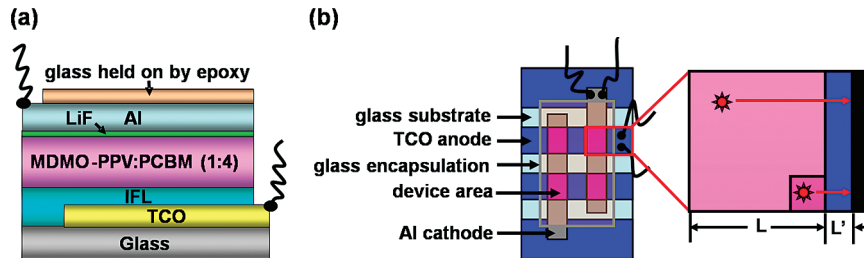


Figure 1. (a) OPV device structure in which the TCO anode is either a commercial ITO or CIO/ITO bilayer film, and the IFL is either PEDOT:PSS or TPDSi₂:TFB; (b) device layout and illustration of charge transfer in TCO anodes.

BHJ OPVs using a poly(2-methoxy-5-(3',7'-dimethyl-octyloxy)-1,4-phenylenevinylene) (MDMO-PPV):[6,6]-phenyl C₆₁ butyric acid methyl ester (PCBM) blend as the active layer. OPV power conversion efficiency (PCE) values of 1.10% and 1.49% are achieved for CIO/ITO-based OPV devices having poly(3,4-ethylenedioxythiopene):poly(styrenesulfonate) (PEDOT:PSS) or 4,4'-bis[(*p*-trichlorosilylpropylphenyl)-phenylamino]-biphenyl:poly[9,9-diethylfluorene-*co*-N-[4-(3-methylpropyl)]-diphenylamine] (TPDSi₂:TFB), respectively, as the anode side interfacial layer (IFL)—indistinguishable from the performance of commercial ITO-based control devices having the same 0.06 cm² device size and fabricated in parallel. The effects of TCO conductivity on OPV performance are systematically analyzed at various device sizes using a simulation model. The results show that CIO/ITO bilayer anodes should significantly outperform ITO in larger area cells.

Experimental Section

TCO Film Fabrication and Characterization. The bilayer TCO components, 170 nm CIO and 35 nm ITO, were consecutively deposited on Corning 1737F glass substrates (2.5 × 2.5 cm) by metal-organic chemical vapor deposition (MOCVD)^{14,15} using bis(1,1,1,5,5-hexafluoro-2,4-pentanedionato)(*N,N*-diethyl-*N'*,*N'*-dimethylethylenediamine)Cd(II) and tris(dipivaloylmethanato)In(III) precursors and ion-assisted deposition (IAD)^{16,17} with an ITO target (In₂O₃:SnO₂ = 9:1) from Williams Advanced Materials Inc., respectively. Commercial ITO substrates (150 nm, ~10.8 Ω/□) were purchased from Delta Technologies, Ltd., in 2.5 × 7.5 cm strips on polished float glass. Film thicknesses were measured with a Tencor P-10 profilometer. Sheet resistance (R_{sheet}) and conductivity were measured with a four-probe Bio-Rad HL5500 van der Pauw Hall-effect instrument. Overall optical transmittance spectra of the TCO samples including the glass substrate were collected with a Cary 500 UV-vis-NIR spectrophotometer. Film elemental compositions were analyzed using inductively coupled plasma atomic emission spectrometry (ICP-AES). Film surface morphologies were characterized by atom force microscopy (AFM) using a

JEOL JSPM-5200 scanning probe microscope operating in the tapping mode.

OPV Device Fabrication and Testing. The present OPV device structure and layout are shown in Figure 1. All TCO substrates were patterned with hot HCl solution, quenched in NaHCO₃ solution, and then cleaned by successive ultrasonication in aqueous detergent, deionized water, methanol, acetone, and isopropanol. For PEDOT:PSS-based devices, TCO substrates were treated with a UV ozone cleaner (Jelight Company Inc., Model 42) for 30 min prior to PEDOT:PSS deposition to remove organic contaminants and to increase the TCO hydrophilicity. Then, a ~40 nm thick PEDOT:PSS (1:6 by weight) film was spin-coated from an aqueous dispersion (H. C. Starck Inc., Baytron P VP AI 4083) and cured in air at 150 °C for 10 min. For TPDSi₂:TFB-based devices, the optimum TCO UVO cleaning time was found to be 5 min. Both TPDSi₂ and TFB were synthesized according to previously published methods.^{18,19} After spin-coating the blended IFL from a toluene precursor solution (2.5 mg/mL of each component) in a N₂ glovebox, the ~10 nm thick films were exposed to air for 5 min to induce cross-linking and were then annealed in the glovebox at 70 °C for 1 h. Highly regioregular MDMO-PPV was synthesized according to the procedure of Mozer et al.²⁰ to achieve optimum charge transport properties and was mixed with PCBM (from American Dye Source Inc.) in a 1:4 weight ratio in distilled chlorobenzene. The blend was then spin-coated onto the IFLs to yield ~100 nm thick active layer films, followed by annealing at 70 °C for 1 h in the glovebox. The OPV performance resulting from MDMO-PPV:PCBM film annealing procedures depends on the polymer microstructure,²¹ and the annealing procedure used here for the regioregular polymer blend was determined experimentally to afford optimum performance. The active layer absorption spectrum was recorded on a Varian Cary 5000 UV-vis-NIR spectrophotometer. LiF/Al (0.6 nm/80 nm) cathodes were subsequently deposited without breaking vacuum by thermal evaporation at ~10⁻⁶ Torr, using a shadow mask to define ~0.2 × 0.3 cm device areas. After encapsulating with a UV-curable epoxy, the OPVs were characterized in ambient at 25 °C using a Class A Spectra-Nova Technologies solar cell analyzer with a Xe lamp and a filter simulating AM 1.5G light in the range 400–1100 nm range at 1000 W/m². The instrument was calibrated using a silicon solar cell fitted with a KG3 filter certified by the National Renewable Energy

- (14) Wang, A.; Babcock, J. R.; Edleman, N. L.; Metz, A. W.; Lane, M. A.; Asahi, R.; Dravid, V. P.; Kannewurf, C. R.; Freeman, A. J.; Marks, T. J. *Proc. Natl. Acad. Sci. U.S.A.* **2001**, *98*, 7113.
- (15) Metz, A. W.; Ireland, J. R.; Zheng, J. G.; Lobo, R.; Yang, Y.; Ni, J.; Stern, C. L.; Dravid, V. P.; Bontemps, N.; Kannewurf, C. R.; Poepelmeier, K. R.; Marks, T. J. *J. Am. Chem. Soc.* **2004**, *126*, 8477.
- (16) Yang, Y.; Huang, Q. L.; Metz, A. W.; Ni, J.; Jin, S.; Marks, T. J.; Madsen, M. E.; DiVenere, A.; Ho, S. T. *Adv. Mater.* **2004**, *16*, 321.
- (17) Li, J. F.; Hu, L. B.; Liu, J.; Wang, L.; Marks, T. J.; Gruner, G. *Appl. Phys. Lett.* **2008**, *93*, 083306.
- (18) Huang, Q. L.; Evmenenko, G. A.; Dutta, P.; Lee, P.; Armstrong, N. R.; Marks, T. J. *J. Am. Chem. Soc.* **2005**, *127*, 10227.
- (19) Yan, H.; Lee, P.; Armstrong, N. R.; Graham, A.; Evmenenko, G. A.; Dutta, P.; Marks, T. J. *J. Am. Chem. Soc.* **2005**, *127*, 3172.
- (20) Mozer, A. J.; Denk, P.; Scharber, M. C.; Neugebauer, H.; Sariciftci, N. S.; Wagner, P.; Lutsen, L.; Vanderzande, D. *J. Phys. Chem. B* **2004**, *108*, 5235.
- (21) Bertho, S.; Janssen, G.; Cleij, T. J.; Conings, B.; Moons, W.; Gadisa, A.; D'Haen, J.; Goovaerts, E.; Lutsen, L.; Manca, J.; Vanderzande, D. *Sol. Energy Mater. Sol. Cells* **2008**, *92*, 753.

Table 1. Properties of the TCO Films

sample	thickness (nm)	R_{sheet} (Ω/\square)	T (%)	Φ^a ($10^{-3} \Omega^{-1}$)	In (atom %)	w_{rms}^b (nm)
CIO	170	5.0	79.5	20.2	4.3	4.7
CIO/ITO	170/35	4.9	79.7	21.1	19	3.7
commercial ITO	150	10.8	85.3	18.9	93	1.5

^aFigure of merit = T^{10}/R_{sheet} . ^brms roughness.

Laboratory (NREL)⁶ so that the spectral mismatch correction factor approaches unity.

Results and Discussion

TCO Characteristics. A 35 nm thick ITO layer was deposited on top of the highly conductive MOCVD-derived CIO films by IAD at room temperature to protect the acid-vulnerable CIO films from corrosion by the acidic PEDOT:PSS. The bilayer films contribute high CIO conductivity, favorable ITO work function and corrosion resistance, a smoother surface morphology, and encapsulation of nonbenign materials with the ITO overcoating.

As summarized in Table 1, the 170 nm thick CIO film has R_{sheet} as low as $\sim 5.0 \Omega/\square$, reflecting the high conductivity, $\sim 13\,000 \text{ S/cm}$, which is significantly greater than that of typical ITO substrates, for example, $\sim 5000 \text{ S/cm}$ for the commercial ITO used in this study. The effective R_{sheet} of the bilayer TCO film can be assumed to be the resistance of the two single layers coupled in parallel. The slightly lower R_{sheet} after ITO deposition (Table 1) indicates good interfacial connectivity between the two layers. The R_{sheet} of the CIO/ITO bilayer is far lower than that of the commercial ITO (4.9 vs $10.8 \Omega/\square$). Figure 2a shows the optical transmittance spectra of the CIO, CIO/ITO bilayer, and commercial ITO films. Compared to the as-grown CIO films, the bilayer film exhibits comparable average transmittance (T , 79.7% vs 79.5%) in the visible range (400–700 nm). The transmittance spectra of the CIO film in the visible range before and after the ITO coating are compared with a typical OPV active layer (MDMO-PPV:PCBM, 100 nm) absorption spectrum in Figure 2b. The transmittance maximum shifts slightly from the red region to the green after the ITO deposition, which can be associated with interference-related changes in the transmittance and reflectance properties of multilayered structures.²² The shift results in a better match of the TCO transmittance with the MDMO-PPV absorption efficiency, which should benefit OPV external quantum efficiency (EQE) and PCE. As summarized in Table 1, compared to ITO, the CIO/ITO bilayer has a slightly lower T but a significantly improved R_{sheet} value. Figure of merit²³ (Φ , $\Phi = T^{10}/R_{\text{sheet}}$) values express the overall TCO film electrical and optical quality. Note that the CIO/ITO bilayer has a higher FOM value than the ITO sample. The In content of the CIO/ITO bilayer was measured to be

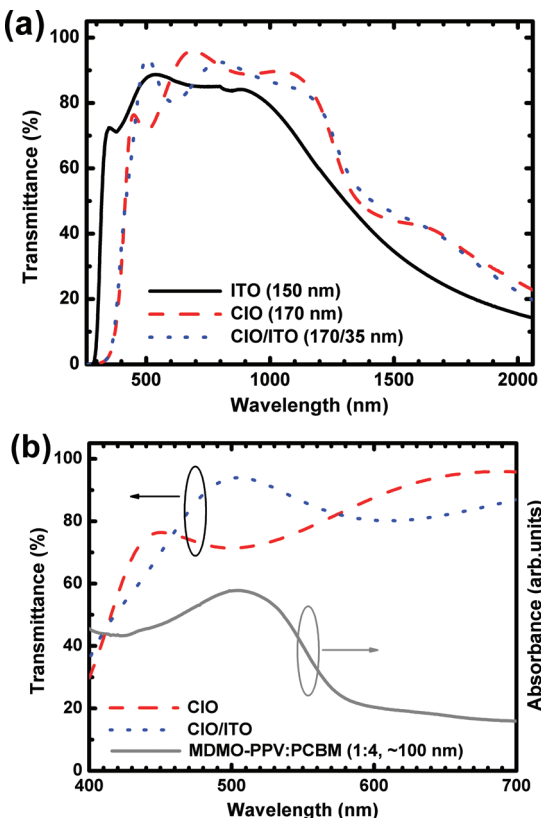


Figure 2. (a) Optical transmittance spectra of the TCO substrates and (b) absorbance spectrum of an MDMO-PPV/PCBM film ($\sim 100 \text{ nm}$) and transmittance spectra of CIO and CIO/ITO bilayer films in the visible range.

~ 19 atom % by ICP-AES, much lower than the > 90 atom % of most commercial ITO films. Such a low In content should effectively lower the raw material costs considering the high price of In compared to Cd (~ 700 vs < 10 US\$/kg).²⁴

Figure 3 shows tapping mode AFM images of the present TCO films. The root-mean-square (rms) roughness of the MOCVD-derived CIO film is $\sim 4.7 \text{ nm}$. The surface becomes slightly smoother after ITO deposition, and the rms roughness decreases to $\sim 3.7 \text{ nm}$, which is still somewhat greater than $\sim 1.5 \text{ nm}$ for the commercial ITO.

OPV Performance Analysis. OPV light and dark current density–voltage ($J - V$) characteristics for each type of device having good reproducibility are shown in Figure 4a,b, respectively. The CIO/ITO-based device using TPDSi₂:TFB as the IFL clearly exhibits a significantly increased open-circuit voltage (V_{oc}), higher short-circuit current density (J_{sc}), larger fill factor (FF), and thus much greater PCE vs the corresponding PEDOT:PSS device. The same trend is also evident for the commercial ITO-based devices because the high-lying TPDSi₂:TFB lowest unoccupied molecular orbital (LUMO) suppresses electron leakage to, and recombination at, the TCO anode.⁷ BHJ OPVs with the same IFLs were fabricated in parallel on both CIO/ITO bilayer and ITO substrates, with performance differences attributable

(22) Heavens, O. S. *Optical Properties of Thin Solid Films*; Dover Publications: New York, 1965.

(23) Haacke, G. J. *Appl. Phys.* **1976**, *47*, 4086.

(24) *Mineral Commodity Summaries 2009*; U.S. Geological Survey, U.S. Government Printing Office: Washington, DC, 2009.

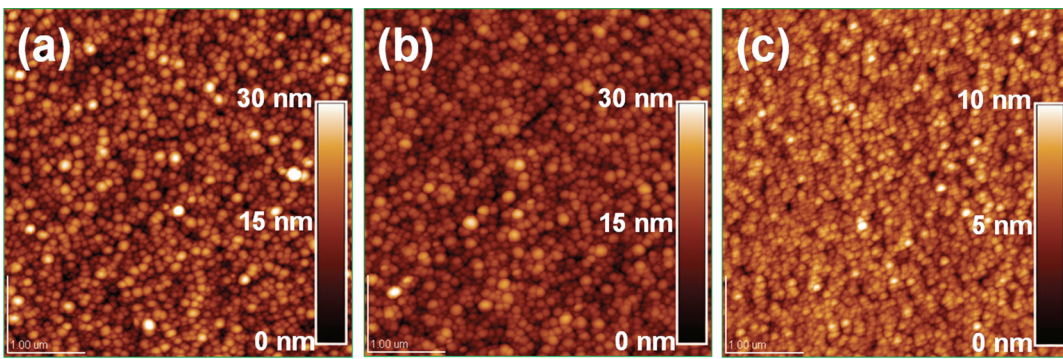


Figure 3. Tapping mode AFM images of (a) CIO, (b) CIO/ITO, and (c) commercial ITO films on glass with $4.5 \times 4.5 \mu\text{m}$ scan areas. The rms roughness values are 4.7, 3.7, and 1.5 nm, respectively.

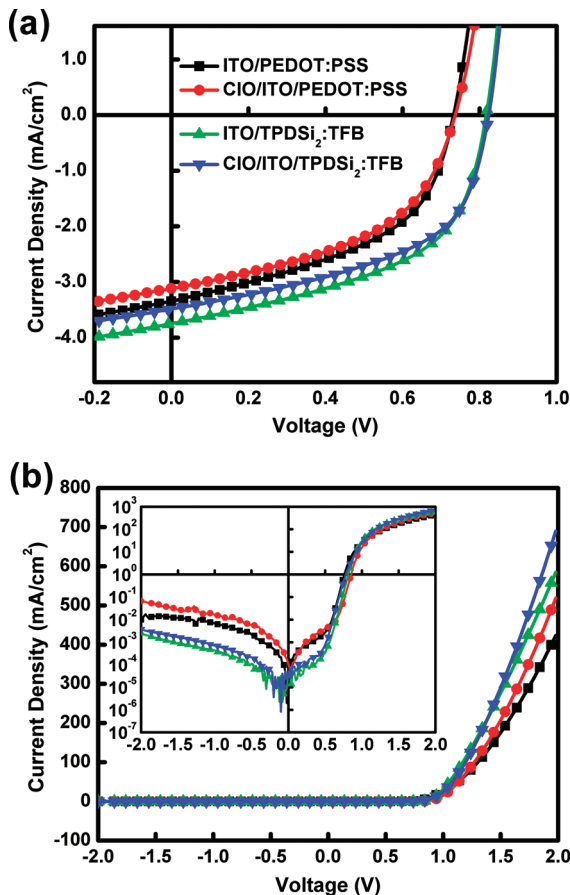


Figure 4. $J-V$ characteristics (a) under 1000 W/m^2 AM 1.5G illumination and (b) in the dark for OPV devices fabricated on the indicated TCO anodes and IFLs and having the architecture glass/TCO/IFL/MDMO-PPV:PCBM/LiF/Al as shown in Figure 1.

to differences in anode characteristics. As seen in Figure 4a and Table 2, the CIO/ITO-based OPVs exhibit V_{oc} values of 0.736 and 0.823 V and FF values of 48.2% and 52.0% for devices using PEDOT:PSS or TPDSi₂:TFB as the IFL, respectively. These response parameters are virtually indistinguishable from those of the corresponding devices fabricated on commercial ITO. Differences in OPV performance may reflect the slightly lower transmittance of the CIO/ITO bilayer vs commercial ITO substrates (Table 1), which would correspondingly decrease the light intensity at the active layer and thus

depress the photocurrent density. To rigorously evaluate TCO transmittance effects on the light intensity at the active layer and thus on OPV performance, the complex optical interference effects should be considered, including the refractive index, extinction coefficient, and thickness of each layer, which ideally should be measured in situ.^{22,25,26} OPV R_s and shunt resistance (R_{sh}) values were calculated from the slopes of the corresponding dark $J-V$ plots at high forward bias and near zero bias, respectively. The measured CIO/ITO-based device R_s values are lower than those of the corresponding ITO-based devices having the same IFL, evident in the greater high-forward-bias slopes in the dark $J-V$ plots (Figure 4b). The R_s values of different devices shown in Figure 4b are compiled in Table 2, with the statistics also showing that the CIO/ITO-based TPDSi₂:TFB devices have lower R_s values than the ITO-based ones (1.28 ± 0.19 vs $1.61 \pm 0.27 \Omega \cdot \text{cm}^2$), consistent with the lower CIO/ITO R_{sheet} ($4.9 \Omega/\square$) vs ITO ($10.8 \Omega/\square$).²⁷ The CIO/ITO-based device R_{sh} values are also lower than those of the ITO-based devices, which together with the slightly lower optical transmittance counterbalances the R_s effect for small devices, resulting in comparable FFs. The lower R_{sh} most likely reflects the higher CIO/ITO film rms roughness ($\sim 3.7 \text{ nm}$ vs $\sim 1.5 \text{ nm}$ for ITO as shown in Figure 3) and possible IFL/active layer morphological differences induced by the increased roughness, which could increase internal loss processes, for example, shorting or carrier recombination.²⁸

TCO Conductivity and Device Area Effects. The R_s of a typical OPV can be divided into two parts as shown in eq 1:

$$R_s = R_{s,\text{electrode}} + R_{s,\text{oht}} \approx R_{s,\text{TCO}} + R_{s,\text{oht}} \quad (1)$$

where $R_{s,\text{electrode}}$ is the R_s arising from the electrodes, including both the metal cathode and the TCO anode,

- (25) Koster, L. J. A.; Mihailescu, V. D.; Xie, H.; Blom, P. W. M. *Appl. Phys. Lett.* **2005**, *87*, 203502.
- (26) Mihailescu, V. D.; Xie, H. X.; de Boer, B.; Koster, L. J. A.; Blom, P. W. M. *Adv. Funct. Mater.* **2006**, *16*, 699.
- (27) Kang, J. W.; Lee, S. P.; Kim, D. G.; Lee, S.; Lee, G. H.; Kim, J. K.; Park, S. Y.; Kim, J. H.; Kim, H. K.; Jeong, Y. S. *Electrochim. Solid-State Lett.* **2009**, *12*, H64.
- (28) Kim, H.; Kushto, G. P.; Auyeung, R. C. Y.; Pique, A. *Appl. Phys. A: Mater. Sci. Process.* **2008**, *93*, 521.

Table 2. OPV Device Performance with Commercial ITO or a CIO/ITO Bilayer as the Anode, PEDOT:PSS or TPDSi₂:TFB as the IFL, and Having the Architecture Glass/TCO/IFL/MDMO-PPV:PCBM/LiF/Al

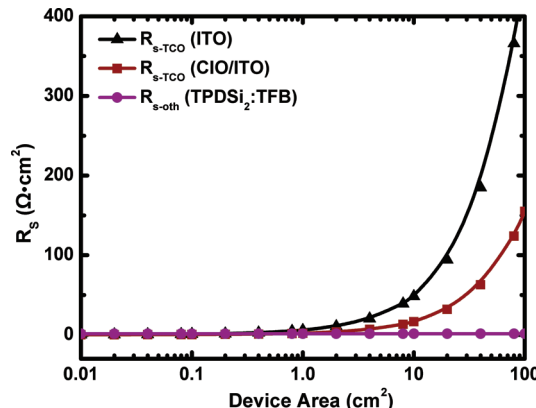
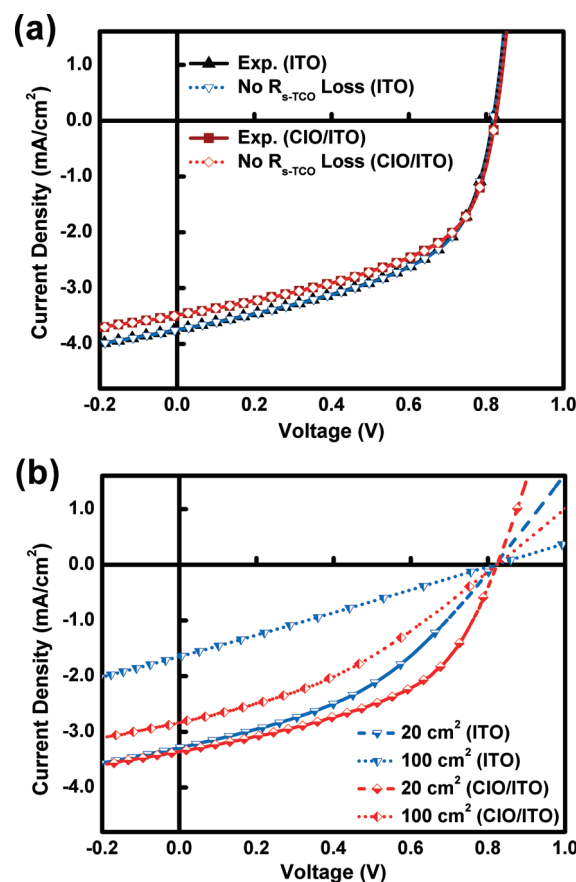
TCO	IFL	<i>V</i> _{oc} (V)	<i>J</i> _{sc} (mA/cm ²)	FF (%)	PCE (%)	<i>R</i> _s ($\Omega \cdot \text{cm}^2$)	<i>R</i> _{sh} ($M\Omega \cdot \text{cm}^2$)	In (atom %)
ITO	PEDOT:PSS	0.732	3.34	48.1	1.18	1.99 (2.06 ± 0.31)	0.34	93
CIO/ITO	PEDOT:PSS	0.736	3.11	48.2	1.10	1.59 (1.66 ± 0.24)	0.23	19
ITO	TPDSi ₂ :TFB	0.817	3.75	51.7	1.58	1.58 (1.61 ± 0.27)	3.27	93
CIO/ITO	TPDSi ₂ :TFB	0.823	3.49	52.0	1.49	1.23 (1.28 ± 0.19)	2.28	19

and $R_{s-\text{oth}}$ contains the contributions from the active layer, interfacial layers, and the interfaces. Since the metal cathode is usually far more conductive ($> 100\times$) than the TCO anode, the resistance arising from the cathode is negligible compared to that from the TCO anode, and thus $R_{s-\text{electrode}}$ in eq 1 can be replaced with $R_{s-\text{TCO}}$. While $R_{s-\text{oth}}$ is independent of the device area due to the perpendicular flow of charge carriers, $R_{s-\text{TCO}}$ increases with the device area because the charge carriers must flow laterally through the TCO anode (Figure 1b). Assuming the device has a square active layer for the convenience of discussion, $R_{s-\text{TCO}}$ can be calculated by

$$R_{s-\text{TCO}} = \frac{L^2}{3\sigma_{\text{TCO}} t_{\text{TCO}}} + \frac{LL'}{\sigma_{\text{TCO}} t_{\text{TCO}}} \quad (2)$$

in which L is the side length of the active layer, L' is the additional distance over which the charge carriers must flow in the TCO before reaching the charge collector (due to the encapsulation, $L' = \sim 0.09$ cm in the current device layout), and σ_{TCO} and t_{TCO} are the TCO film conductivity and thickness, respectively.²⁹ Given the experimental R_s values (Table 2), the conductivities and thicknesses of the commercial ITO (5000 S/cm, 150 nm) and the CIO of the bilayer film (13 000 S/cm, 170 nm), the $R_{s-\text{oth}}$ and $R_{s-\text{TCO}}$ values at various device active areas ($A = L^2$) can be calculated with eqs 1 and 2 and are plotted in Figure 5 for OPVs using TPDSi₂:TFB as the IFL and either ITO or a CIO/ITO bilayer as the anode. For the present laboratory-scale device with $L = 0.2$ cm, $R_{s-\text{TCO}}$ values for the ITO and CIO/ITO bilayer are 0.53 and 0.18 $\Omega \cdot \text{cm}^2$, respectively. As shown in Figure 5, while $R_{s-\text{oth}}$ stays constant at $\sim 1.05 \Omega \cdot \text{cm}^2$, note that $R_{s-\text{TCO}}(\text{ITO})$ increases much more rapidly with device area than does $R_{s-\text{TCO}}(\text{CIO/ITO})$, and this difference becomes even larger as the device area increases.

J–V plots for devices of different areas can be generated by accounting for the voltage losses on the TCO as recently reported,²⁹ using the $R_{s-\text{TCO}}$ data calculated from eq 2. Figure 6a shows simulated results for the TPDSi₂:TFB-based devices with no loss due to the $R_{s-\text{TCO}}$, with the experimental results also plotted for reference. There is no obvious difference between the simulated light *J–V* response and the experimental data for either the ITO- or the CIO/ITO-based devices because of the small R_s and the low $R_{s-\text{TCO}}$ compared to $R_{s-\text{oth}}$ (e.g., 0.53 and 0.18 vs $1.05 \Omega \cdot \text{cm}^2$). Thus, there is very little resistance loss at the TCOs for the present small experimental device size. Figure 6b next shows the simulated results for ITO- and

**Figure 5.** Dependence of series resistance (R_s) on device dimensions.**Figure 6.** Simulated device performance of the TPDSi₂:TFB-based devices using either ITO or CIO/ITO anodes assuming (a) no $R_{s-\text{TCO}}$ -derived power loss and (b) 20 and 100 cm^2 device areas.

the CIO/ITO-based devices having larger areas, 20 and 100 cm^2 , respectively, and the derived device performance parameters are summarized in Table 3. The CIO/ITO-based devices exhibit substantially superior device

(29) Servaites, J. D.; Yeganeh, S.; Marks, T. J.; Ratner, M. A. Efficiency Enhancement in Organic Photovoltaic Cells: Consequences of Optimizing Series Resistance. *Adv. Funct. Mater.*, in press.

Table 3. Simulated OPV Device Performance for Different Device Areas ($A = L^2$) Having TPDSi₂:TFB as the IFL and either Commercial ITO or a CIO/ITO Bilayer as the Anode

TCO	A (cm ²)	R_s (Ω·cm ²)	V_{oc} (V)	J_{sc} (mA/cm ²)	FF (%)	PCE (%)	$\gamma_{p\text{-loss}} (\%)$
ITO	0	1.05	0.817	3.75	51.7	1.58	0
	0.04 ^a	1.58	0.817	3.75	51.7	1.58	0.2
	10	49.4	0.817	3.51	45.3	1.30	18
	20	95.4	0.817	3.28	40.1	1.07	32
	100	458	0.817	1.65	25.2	0.34	78
CIO/ITO	0	1.05	0.823	3.49	52.0	1.49	0
	0.04 ^a	1.23	0.823	3.49	52.0	1.49	0.1
	10	17.5	0.823	3.42	50.1	1.41	5.4
	20	33.1	0.823	3.36	48.1	1.33	11
	100	156	0.823	2.83	35.6	0.83	44

^a Corresponding to experimental device size, where $L = 0.2$ cm.

performance compared to the ITO-based devices—not only having larger FFs, but also higher values of J_{sc} and thus PCE. For 20 cm² area devices, the PCE values are 1.07% and 1.33% for the ITO- and CIO/ITO-based devices, respectively, while at 100 cm² area, these values are 0.34% and 0.83%, respectively. As the device area increases, the difference in device performance between OPVs utilizing ITO vs CIO/ITO bilayer anodes becomes more significant, underscoring the attraction of employing a high-conductivity TCO to suppress the resistive power loss.

PCE values for different OPV areas for all four types of devices examined, descriptively designated “ITO/PEDOT:PSS”, “CIO/ITO/PEDOT:PSS”, “ITO/TPDSi₂:TFB”, and “CIO/ITO/TPDSi₂:TFB” to indicate the corresponding component TCO and IFL materials, are extracted from the simulated $J-V$ plots. Power loss ratio ($\gamma_{p\text{-loss}}$) values originating from the TCO resistances at different device areas are calculated from

$$\gamma_{p\text{-loss}}(A) = \frac{\text{PCE}(0) - \text{PCE}(A)}{\text{PCE}(0)} \quad (3)$$

in which PCE(0) is the PCE for an ideal device with an area of 0, where $R_{s\text{-TCO}} = 0$, and PCE(A) is the PCE for a device with area of A . As summarized in Table 3, the $\gamma_{p\text{-loss}}$ values are only ~0.1% and 0.2% for the experimental sized CIO/ITO- and ITO-based TPDSi₂:TFB OPV devices, respectively. Also calculated with this simulation model, the $\gamma_{p\text{-loss}}$ values are ~0.6% for both the 0.8 cm² CIO/ITO-based and the 0.2 cm² ITO-based TPDSi₂:TFB OPV devices, where the R_s and the $R_{s\text{-TCO}}$ values are ~2.6 and 1.5 Ω·cm², respectively. The result suggests that for small-area devices where R_s values are small (e.g., < 3 Ω·cm²), the change in the fourth quadrant of OPV light $J-V$ plots can be quite minor even while substantial difference may exist in R_s . As shown in Figure 7, the PCE of the commercial ITO-based devices drops far more rapidly than that of the CIO/ITO-based devices as the device area increases, regardless of the IFL, resulting in significantly higher $\gamma_{p\text{-loss}}$ values for the ITO-based devices than for the CIO/ITO-based devices of the same size. The benefits

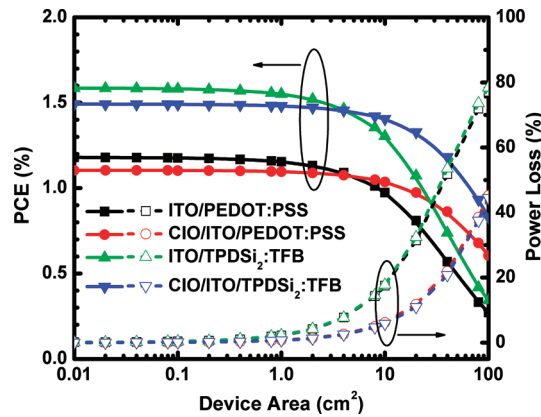


Figure 7. Dependence of device PCE and the $R_{s\text{-TCO}}$ -derived power loss on device area.

of using a high-conductivity TCO are realized in larger cells (> 10 cm²) where the $R_{s\text{-TCO}}$ is larger, as is the $\gamma_{p\text{-loss}}$. It is important to note here that the $R_{s\text{-TCO}}$ and the $\gamma_{p\text{-loss}}$ can be efficiently suppressed by employing a TCO with a higher conductivity than ITO, and this procedure is essential for enhancing device PCE, especially for large-area devices.

Conclusions

Low-indium-content, high-conductivity, transparent bilayer CIO/ITO thin films were fabricated and implemented as anodes in MDMO-PPV:PCBM BHJ OPVs. The CIO/ITO-based devices exhibit performance comparable to that of devices fabricated on commercial ITO substrates for laboratory-scale device sizes using either a PEDOT:PSS or TPDSi₂:TFB as the IFL. The effects of TCO transmittance and conductivity were systematically studied with a simulation model. These results indicate that CIO/ITO bilayer anodes with comparable transmittances and significantly higher conductivities than typical commercial ITO substrates impart substantial advantages to OPV devices, especially for device areas larger than 10 cm².

Acknowledgment. We thank BP Solar and the Northwestern University MRSEC (NSF Grant DMR-0520513) for support of this research.